

The characteristics of granular-bright facet in hydrogen pre-charged and uncharged high strength steels in the very high cycle fatigue regime

Y. D. Li · S. M. Chen · Y. B. Liu · Z. G. Yang ·
S. X. Li · W. J. Hui · Y. Q. Weng

Received: 19 May 2009 / Accepted: 29 October 2009 / Published online: 12 November 2009
© Springer Science+Business Media, LLC 2009

Abstract In this study, the effect of hydrogen on fatigue strength of high strength steels in the very high cycle fatigue regime was further discussed. It is found that the calculated results of fatigue strength by modified Murakami's expression are in good accordance with the experimental results in $\pm 15\%$ error band. The relationship between fatigue life (N_f) and the ratio of granular-bright facet (GBF) to inclusion size $\left(\frac{\sqrt{A_{GBF}}}{\sqrt{A_{inc}}}\right)$ for quenching and tempering (QT) specimens and pre-charged specimens by soaking (SK) and cathodic (CD) charging can be approximately expressed by $\frac{\sqrt{A_{GBF}}}{\sqrt{A_{inc}}} = \frac{R_{GBF}}{R_{inc}} = 0.25N_f^{0.125}$; however, the value of $\frac{\sqrt{A_{GBF}}}{\sqrt{A_{inc}}}$ for specimens pre-charged by high-pressure thermal hydrogen charging is obviously greater than that for QT specimens and pre-charged specimens by SK and CD charging at an identical N_f . The stress intensity factor range at the periphery of the GBF, ΔK_{GBF} , was calculated in this work. It is found that the value of ΔK_{GBF} is not a constant but approximately proportional to $(\sqrt{A_{GBF}})^{1/3}$. Besides it is also found that ΔK_{GBF} decreases with the increase of hydrogen content.

Introduction

For high strength steels, the fatigue crack generally initiates from inner inclusion for specimens having a longer

fatigue life ($>10^7$ cyc) [1–7], and there exists an area with particular morphology beside the inclusion at the fracture origin. The particular morphology looked optically dark when observed by an optical microscope (OM) and it was named the optically dark area (ODA) [2–4]. On the other hand, a white-bright facet area was found in the vicinity of inclusion at the fracture origin by scanning electron microscopy (SEM) observation. This area revealed a very rough and granular morphology in comparison with the area in the fish-eye; therefore, it was named the granular-bright facet (GBF) [5, 6]. Further, it was verified that the size of GBF is the same as that of ODA. It was reported that in the very high cycle fatigue (VHCF, $>10^7$ cyc) regime more than 90% of fatigue life was attributed to the creation of the ODA/GBF. It was pointed out that the formation of the ODA/GBF during the long fatigue process controls the internal fracture mode and ODA/GBF was considered to play a crucial role in the failure mechanism in the VHCF regime [2–4].

Although the formation mechanism of GBF (in this article, we observed the fatigue crack origins by SEM, hence the term GBF is adopted hereafter) is always being investigated, it is still not quite clear until now [2–7]. Murakami considered that the formation of GBF was related to hydrogen trapped by inclusion [2–4]. Hydrogen trapped by inclusion was observed by secondary ion mass spectroscopy (SIMS) [4] and high-resolution tritium autoradiography [8]. Hydrogen embrittlement (HE) is a long-standing subject especially for ferrous alloys [9], it has been studied for almost a century. Hydrogen damage, delayed fracture, and stress corrosion etc. were widely investigated by many researchers; nevertheless, the influence of hydrogen on fatigue properties of high strength steels, particularly, the role of hydrogen in the VHCF regime was not widely studied.

Y. D. Li (✉) · S. M. Chen · Y. B. Liu · Z. G. Yang · S. X. Li
Shenyang National Laboratory for Materials Science,
Institute of Metal Research, Chinese Academy of Sciences,
110016 Shenyang, People's Republic of China
e-mail: ydli@imr.ac.cn

W. J. Hui · Y. Q. Weng
Central Iron and Steel Research Institute,
100081 Beijing, People's Republic of China

In the present article, the influence of hydrogen on fatigue properties of high strength steels was investigated through pre-charging several high strength steels with different hydrogen charging technologies, the emphasis was placed on the characteristics of GBF.

Materials and experiments

Seven high strength steels (including four kinds of spring steels: G50CrV4, F50CrV4, SUP12, and 60Si2CrV; three kinds of bearing steels: GER, GVM, and G) were prepared in the experiment, their chemical compositions (mass%) are shown in Table 1, and their heat treatment procedures (quenching and tempering, QT) are shown in Table 2. The nominal chemical compositions of G50CrV4 and F50CrV4 are the same, however, the latter is clean steel and the inclusion size is much smaller. GER and GVM were the bearing steels with same nominal compositions, but GER was treated by electroslag remelting (ER) and GVM was treated by vacuum melting (VM). G was supposed to be as a bearing steel, it was also treated by VM and the oxygen content was reduced to 6–7 ppm, but during the deoxidation process the carbon content was removed severely as well. The microstructures of these steels were all tempered martensite after QT. The dimension of fatigue specimens is shown in Fig. 1, and the length of specimen's shoulder, d , depended on Young's modulus and density, is about 10 mm. In order to decrease the influence of surface roughness as much as possible, the surface on the mid-

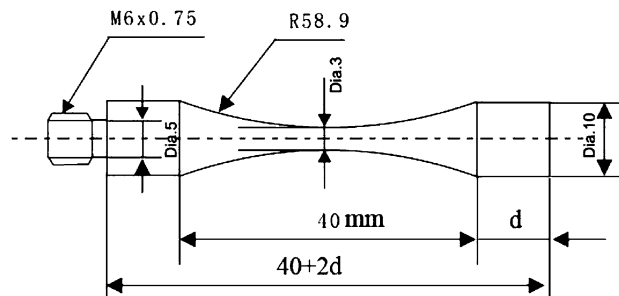


Fig. 1 Dimension of the fatigue sample used in very high cycle fatigue testing

section of specimens was polished with grades 600, 800, 1000, 1200 abrasive papers consecutively after QT.

In order to investigate the influence of hydrogen on fatigue properties, hydrogen is charged into some specimens after QT. Charging technologies used in present work include the cathodic (CD) charging, the soaking (SK), and high-pressure thermal hydrogen charging (HPTHC). The solution used for the CD charging was 3% NaCl + 3 g/L NH_4SCN aqueous solution, at different current densities for 6 h; the solution used for SK was a 20 mass% ammonium thiocyanate solution (NH_4SCN), at the charging temperature of 288 K for 24 or 48 h. After the CD charging, the specimens were coated with cadmium to prevent hydrogen desorption, and then the pre-charged specimens were placed at ambient temperature for 12 h in order to homogenize the hydrogen distribution in the specimens. After SK, the specimens were placed at ambient temperature for 1.5 h. For specimens pre-charged by the CD charging, the cadmium coating is removed before measuring hydrogen content. The HPTHC facility used in this work was set up by the Institute of Metal Research. In this HPTHC experiment, the temperature was 573 K, the hydrogen pressure was 10^7 Pa (the purity of hydrogen was 99.999%), the time for hydrogen charging was 5 days. Some F50CrV4 specimens were annealed at 653 K for 4 h in a vacuum after QT in order to release the hydrogen trapped by inclusions. The total hydrogen content was determined by the RH-404 Hydrogen Determinator (accuracy: 0.02 ppm). The symbols of all pre-charged and uncharged specimens, the conditions of hydrogen charging

Table 1 The chemical compositions of all steels (mass%)

| Steel | C | Mn | Si | S | P | Cr | V | Al |
|---------------------|------|------|------|--------------|--------------|------|------|-------|
| F50CrV4/ G50CrV4 | 0.51 | 0.95 | 0.30 | ≤ 0.015 | ≤ 0.015 | 1.10 | 0.13 | 0.02 |
| SUP12 | 0.53 | 0.69 | 1.49 | 0.007 | 0.011 | 0.74 | – | 0.039 |
| 60Si2CrV | 0.59 | 0.60 | 1.6 | 0.006 | 0.009 | 1.09 | 0.11 | 0.013 |
| GER | 1.22 | 0.33 | 0.40 | 0.002 | 0.008 | 1.49 | – | – |
| GVM | 1.20 | 0.31 | 0.34 | 0.011 | 0.016 | 1.72 | – | – |
| G | 0.24 | 0.77 | 0.45 | 0.001 | 0.012 | 1.2 | – | – |

Table 2 The heat treatment procedures of all steels

| Steels | QT procedures | Vickers hardness, HV (kgf/mm^2) |
|-----------------|---|---|
| F50CrV4/G50CrV4 | 860 °C, 30 min + O.Q. + 440 °C, 1 h + A.C. | 440/450 |
| 60Si2CrV | 920 °C, 15 min + O.Q. + 430 °C, 30 min + W.C. | 565 |
| SUP12 | 845 °C, 30 min + A.C. + 845 °C, 30 min + O.Q. + 430 °C, 60 min + W.C. | 600 |
| GER/GVM | 860 °C, 20 min + O.Q. + 180 °C, 2 h + A.C. | 708/703 |
| G | 860 °C, 10 min + O.Q. + 180 °C, 2 h + A.C. | 414 |

Table 3 The symbols and hydrogen charging conditions for fatigue test specimens

| Steel | Symbol of specimens | Charging method | Charging time | Experimental temperature | Hydrogen content of uncharged specimens (ppm) | Hydrogen content of pre-charged specimens (ppm) |
|----------|---------------------|----------------------------------|---------------|--------------------------|---|---|
| G50CrV4 | G-QT | Uncharged | – | – | 0.66 | – |
| | G-SK1 | Soaking | 24 h | 288 K | 0.66 | 2.0 |
| | G-SK2 | Soaking | 48 h | 288 K | 0.66 | 3.0 |
| F50CrV4 | F-VA | Uncharged | – | – | 0.2 | – |
| | F-QT | Uncharged | – | – | 0.6 | – |
| | F-HPTHC | HPTHC | 5 days | 573 K | 0.6 | 2.5 |
| 60Si2CrV | SCV-QT | Uncharged | – | – | 0.15 | – |
| | SCV-HPTHC | HPTHC | 5 days | 573 K | 0.15 | 3.0 |
| | SCV-CD1 | Cathodic, 1 mA/cm ² | 6 h | Room temperature | 0.15 | 3.2 |
| | SCV-CD2 | Cathodic, 2 mA/cm ² | 6 h | Room temperature | 0.15 | 10.0 |
| SUP12 | SUP-QT | Uncharged | – | – | 0.27 | – |
| | SUP-CD | Cathodic, 0.6 mA/cm ² | 6 h | Room temperature | 0.27 | 1.0 |
| | SUP-HPTHC | HPTHC | 5 days | 573 K | 0.27 | 2.0 |
| GER | GER | Uncharged | – | – | 0.4 | – |
| GVM | GVM | Uncharged | – | – | 0.4 | – |
| G | G | Uncharged | – | – | 0.28 | – |

VA vacuum annealing

for all steels and the hydrogen contents of uncharged and pre-charged specimens are shown in Table 3.

The ultrasonic fatigue testing was conducted on a Shimadzu USF-2000 testing system with a resonance frequency of 20 kHz, resonance interval of 150 ms at a load ratio of $R = -1$. All experiments were tested at room temperature in air. The fatigue specimens were cooled by compressive air during testing. The tensile testing was conducted on an Instron 8801 machine, with the tensile strain rate of 10^{-3} /s. All fracture surfaces were observed by using the Quanta 600 scanning electron microscopy.

Experimental results

Tensile and fatigue experiments

The tensile properties for all specimens are shown in Table 4. It can be easily found that the pre-charged specimens show lower ultimate tensile strength and lower elongation. Figure 2 shows the contrastive tensile curves of some pre-charged and uncharged specimens, and we can find that hydrogen charging reduces the elongation apparently and ultimate tensile strength noticeably no matter what charging method is applied; however, hydrogen charging changes hardly the Young's modulus. Figures 3 and 4 show the tensile fractographs of some uncharged and pre-charged specimens. On the fracture surface of uncharged specimen,

it shows a great many dimples (Figs. 3a, 4a), but after being pre-charged the fracture surface becomes intergranular and cleavage fracture (Figs. 3b, c, 4b–d).

In each fatigue test, at least 14 specimens were used to determine the fatigue strength by staircase method. The fatigue strengths of all specimens at 10^9 cyc were listed in Table 4, and $S-N$ curves were shown in Fig. 5 [10]. It is obvious that hydrogen charging can reduce the fatigue strength at 10^9 cyc significantly. Fatigue fractographs of all specimens were observed by SEM. Almost all the specimens were failed from inner defects. The internal crack initiation sites were mostly inclusion clusters for F50CrV4 steel [11] (see Fig. 6a, b), these clusters were composed of small inclusions, and electron probe microelement analysis (EPMA) revealed the constituents of these small inclusions (MnS, carbide, and oxide). Each inclusion in the cluster is very small, the size is about 2–3 μm , which is smaller than the critical size for a single inclusion to initiate a fatigue crack [12], however, the equivalent size of inclusion cluster is greater than the critical size. The equivalent size of inclusion cluster is about 6 μm by measuring clear fractographs of some specimens. Except F50CrV4 steel, almost all steels were failed from internal single inclusions. The single inclusion was mainly Ca duplex inclusion ($\text{CaO}\cdot\text{Al}_2\text{O}_3$, $\text{CaO}\cdot\text{Al}_2\text{O}_3\cdot\text{MgO}$) (see Fig. 6c, d) or occasionally TiN. It was observed by SEM that there was a bright rough area beside the inclusion in specimens with longer life, this was the granular-bright facet (GBF) area [5, 6]. The inclusion size at the fracture origins was

Table 4 The tensile properties and fatigue properties of all specimens

| Steel | Symbol of specimens | C_r (ppm) | C_i (ppm) | Ultimate tensile strength, σ_b (MPa) | Elongation (%) | Average inclusion size, $\sqrt{A_{inc}}$ (μm) | Fatigue strength at 10^9 cyc |
|----------|---------------------|-------------|-------------|---|----------------|--|--------------------------------|
| G50CrV4 | G-QT | 0 | 0.66 | 1,550 | 14.5 | 30.6 | 571 |
| | G-SK1 | 1.34 | 0.66 | 1,500 | 3.6 | 34.3 | 467 |
| | G-SK2 | 2.34 | 0.66 | 1,470 | 3 | 37.3 | 366 |
| F50CrV4 | F-VA | 0 | 0.2 | 1,540 | 15 | $\sim 6^a$ | 713 |
| | F-QT | 0 | 0.6 | 1,529 | 14 | $\sim 6^a$ | 703 |
| | F-HPTHC | 0 | 2.5 | 1,488 | 13 | $\sim 6^a$ | 498 |
| 60Si2CrV | SCV-QT | 0 | 0.15 | 2,365 | 18 | 16.4 | 767 |
| | SCV-HPTHC | 0 | 3.0 | 1,750 | 4 | 11.3 | 392 |
| | SCV-CD1 | 0.15 | 3.05 | 1,630 | 4.7 | 20.5 | 483 |
| | SCV-CD2 | 0.15 | 9.85 | 1,452 | 3.8 | 18.9 | 497 |
| SUP12 | SUP-QT | 0 | 0.27 | 1,815 | 17 | 17.4 | 771 |
| | SUP-CD | 0.73 | 0.27 | 1,800 | 10 | 18.0 | 628 |
| | SUP-HPTHC | 0 | 2 | 1,847 | 8 | 14.1 | 413 |
| GER | GER | 0 | 0.4 | 1,700 | – | 11.4 | 788 |
| GVM | GVM | 0 | 0.4 | 1,785 | – | 23.3 | 746 |
| G | G | 0 | 0.28 | 1,489 | 18 | 26.5 | 601 |

^a The equivalent inclusion cluster size

Fig. 2 Tensile curves of some pre-charged and uncharged specimens. **a** G50CrV4, **b** F50CrV4

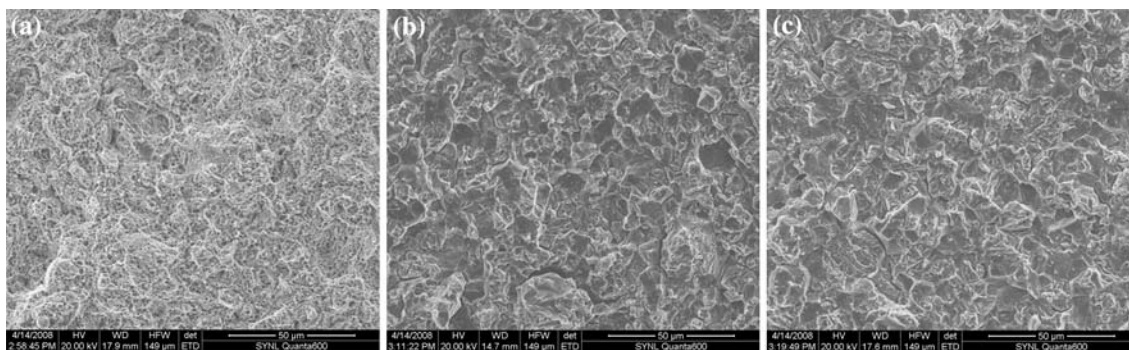
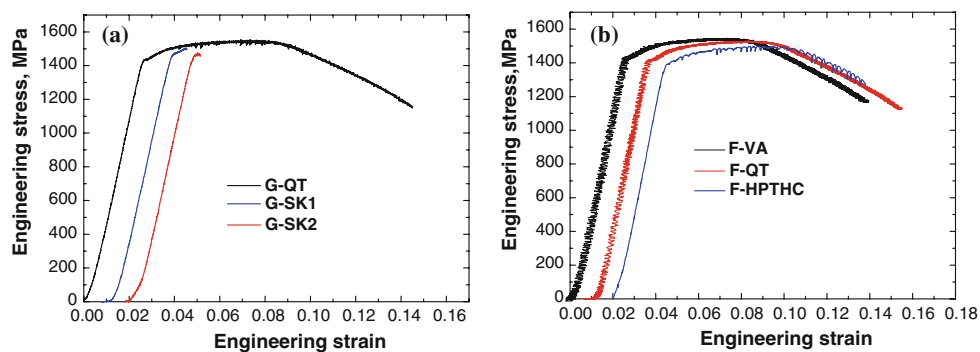
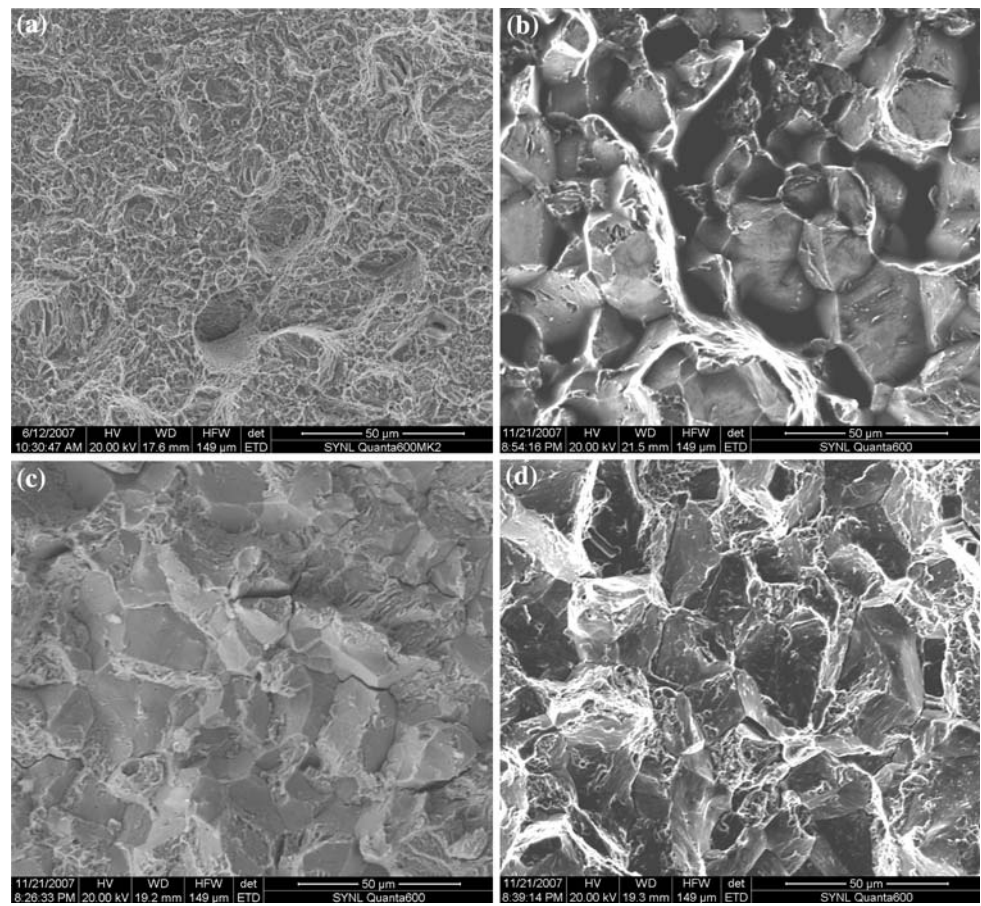


Fig. 3 The tensile fractographs of G50CrV4 steels; **a** G-QT, **b** G-SK1, **c** G-SK2

measured and the average inclusion size at fracture origins for each kind specimen (the equivalent cluster size is measured for F50CrV4 steels) was obtained by statistics

and was listed in Table 4. Usually the nonmetallic inclusion at the fracture origin is considered to be the largest inclusion in the gauge section of a specimen [13] and the

Fig. 4 Tensile fractographs of 60Si2CrV steel; **a** specimen SCV-QT, **b** specimen SCV-HPTHc, **c** specimen SCV-CD1, **d** specimen SCV-CD2



maximum inclusion size obtained by metallographic observation is usually much smaller than the maximum inclusion size measured on the fracture surface.

Discussion

The fatigue strength influenced by hydrogen

In our previous article [10], the fatigue strength expression of Murakami was modified to Eq. 1 after considering the influence of hydrogen.

$$\sigma_{w*} = f(C) \frac{1.56(HV + 120)}{(\sqrt{A_{inc}})^{1/6}} \tag{1}$$

where C is hydrogen content, $f(C)$ the hydrogen influence factor, and $f(C) \leq 1$, σ_{w*} the fatigue strength after considering hydrogen influence; HV Vickers hardness, in kgf/mm^2 ; and $\sqrt{A_{inc}}$ the square root of projective area of inclusion, in μm . In the previous article [10], we discussed the classification of diffusible hydrogen (trapped by reversible traps, such as dislocation, vacancy, crystal lattice) and non-diffusible hydrogen (trapped by irreversible traps, such as inclusion, void, etc.) through different hydrogen charging

methods. Hydrogen in specimens F-VA, F-QT, F-HPTHc, SCV-QT, SCV-HPTHc, G-QT, SUP-QT, and SUP-HPTHc can be mainly classified into non-diffusible hydrogen and hydrogen being charged into specimens SCV-CD1, SCV-CD2, G-SK1, G-SK2, and SUP-CD can be mainly classified to diffusible hydrogen. The expression of $f(C)$ for diffusible hydrogen and non-diffusible hydrogen are respectively as follows [10]:

$$f(C_r) = 0.6 + 0.4 \exp(-C_r^2/4), \tag{2}$$

$$f(C_i) = \frac{1}{1 + 0.09C_i^2}, \tag{3}$$

where C_r is the diffusible hydrogen content (ppm), and C_i is the non-diffusible hydrogen content. The total hydrogen content (C_H) was considered as the sum of diffusible hydrogen content and non-diffusible hydrogen content, $C_H = C_r + C_i$. The diffusible hydrogen content (C_r) and non-diffusible hydrogen content (C_i) for each specimen are listed in Table 4. In general, Vickers hardness of high strength steels is less sensitive to hydrogen charging unless geometric softening caused by voids and fissures at severe charging conditions happened [14, 15]. Reference [10] provided some HV values of pre-charged and uncharged high strength steels in which it shows that the HV values are

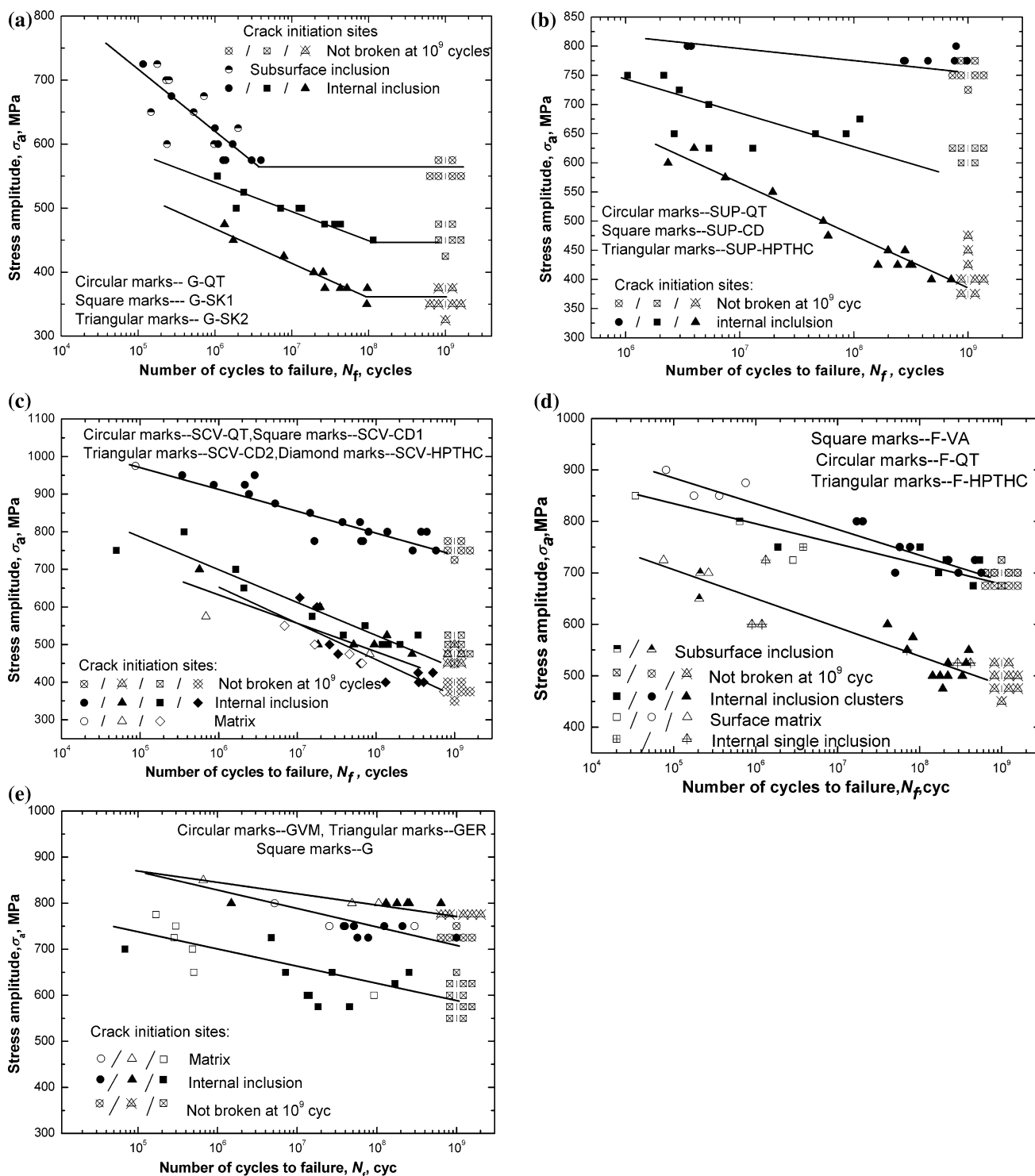
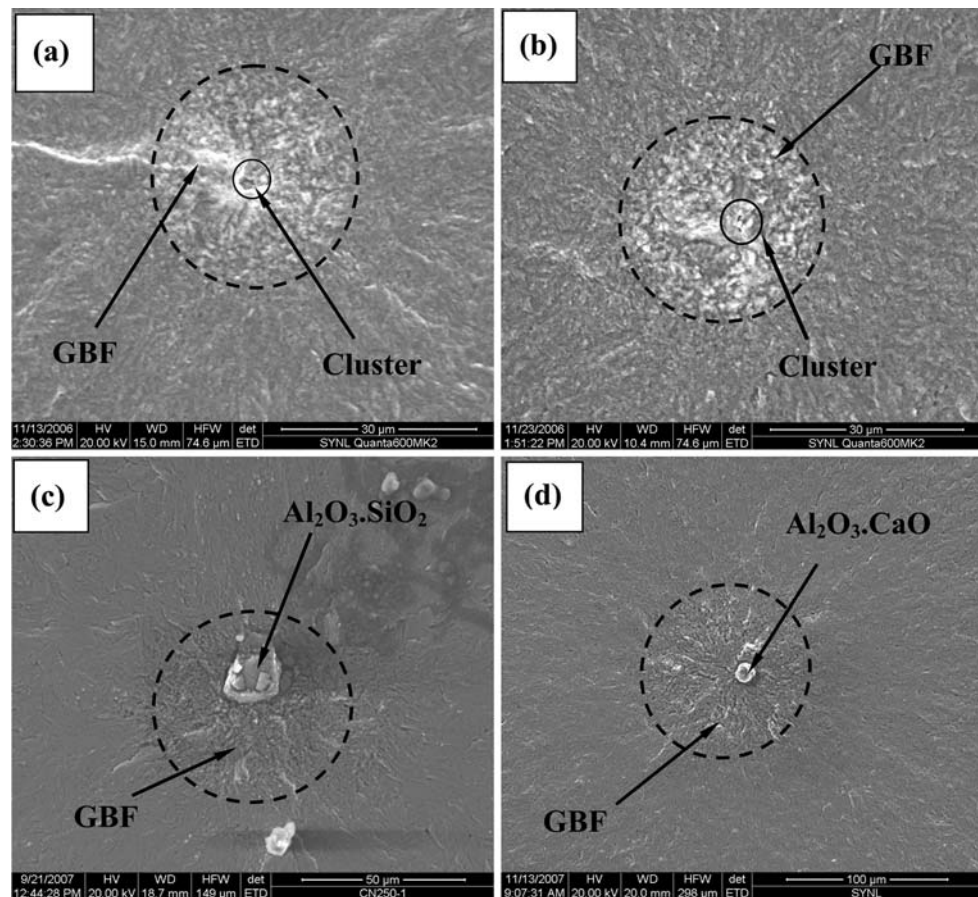


Fig. 5 S - N curves of all pre-charged and uncharged specimens; **a** G50CrV4 [10], **b** SUP12 [10], **c** 60Si2CrV [10], **d** F50CrV4, and **e** GCr15 (including G, GVM, and GER)

not sensitive to hydrogen charging indeed. Therefore, in the present article, Vickers hardness of pre-charged specimens is considered to be the same as uncharged specimens, and the HV of uncharged steels is listed in Table 2. For specimens SCV-CD1, SCV-CD2, G-SK1, G-SK2, and SUP-CD,

the influence of non-diffusible hydrogen can be ignored. Substituting diffusible hydrogen content (C_r) into Eq. 2 and substituting Eq. 2 into Eq. 1, then the calculated fatigue strengths— $\sigma_{w,cal}^*$ will be obtained. In a similar way, the calculated fatigue strengths for specimens F-VA, F-QT,

Fig. 6 The fatigue fracture origins observed by SEM: **a** F-VA specimen, **b** F-QT specimen [11], **c** SCV-CD1 specimen [10], and **d** SUP-HPTHC specimen. Fracture condition: **a** $\sigma_a = 725$ MPa, $N_f = 2.13 \times 10^8$; **b** $\sigma_a = 725$ MPa, $N_f = 2.26 \times 10^8$; **c** $\sigma_a = 525$ MPa, $N_f = 1.39 \times 10^8$; **d** $\sigma_a = 450$ MPa, $N_f = 1.99 \times 10^8$



F-HPTHC, SCV-QT, SCV-HPTHC, G-QT, SUP-QT, and SUP-HPTHC will be easily obtained. In the process of calculating $\sigma_{W,cal}^*$, the average inclusion sizes or the equivalent cluster sizes at the fatigue fracture origins in Table 4 are used.

The calculated fatigue strengths— $\sigma_{W,cal}^*$ and the experimental values— $\sigma_{W,exp}^*$ were compared in Fig. 7 in which $\sigma_{W,cal}^*$ and $\sigma_{W,exp}^*$ were normalized with $(HV + 120)$. It is found that the calculated results were in good accordance with the experimental values for these specimens, which indicates the validity of Eqs. 1–3.

The relationship between fatigue life and the size of GBF

It was pointed out that the formation of GBF during the long fatigue process controls the internal fracture mode and GBF was considered to play a crucial role in the failure mechanism in the VHCF regime [2–7]. More than 90% of fatigue life was attributed to the creation of the GBF. However, the formation mechanism of GBF has not yet to be elucidated very clearly. It was assumed by Murakami that the GBF is made by cyclic fatigue stress and the

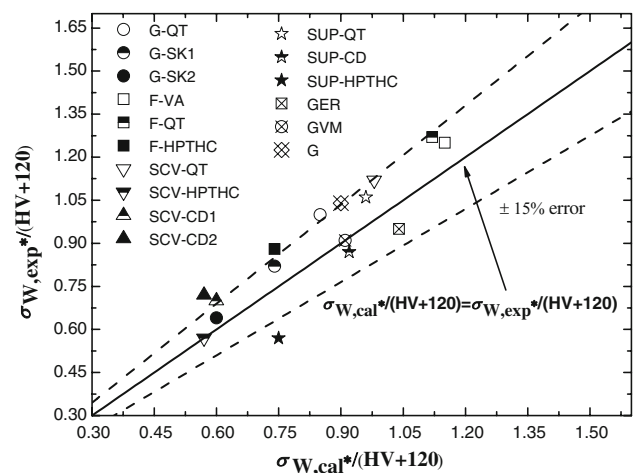


Fig. 7 The comparison of calculated fatigue strength with experimental results

synergetic effect of hydrogen, which is trapped by the inclusion at the fracture origin. And Murakami concluded through experiments that hydrogen trapped by inclusion is a crucial factor, which causes the VHCF failure of high strength steels [3, 4].

Generally the size of GBF increases with an increase in fatigue life. Chapetti et al. [16] obtained the empirical relationship between fatigue life (N_f) and the ratio of GBF to inclusion size ($\frac{\sqrt{A_{GBF}}}{\sqrt{A_{inc}}}$) through collecting some experimental results in references [5, 17–19]. The expression describing the relationship between N_f and $\frac{\sqrt{A_{GBF}}}{\sqrt{A_{inc}}}$ is as follows [16]:

$$\frac{\sqrt{A_{GBF}}}{\sqrt{A_{inc}}} = \frac{R_{GBF}}{R_{inc}} = 0.25N_f^{0.125}, \quad (4)$$

where $\sqrt{A_{GBF}}$ and $\sqrt{A_{inc}}$ are, respectively, the sizes of GBF and inclusion defined by Murakami, and R_{GBF} and R_{inc} are, respectively, the radii of GBF and inclusion. In this article, the inclusion size is included in GBF size. These experimental results collected by Chapetti are all from QT high strength steels.

Equation 4 can be rewritten as:

$$N_f = 6.5 \times 10^4 \left(\frac{R_{GBF}}{R_{inc}} \right)^8. \quad (5)$$

In this work, the relationship between N_f and $\frac{\sqrt{A_{GBF}}}{\sqrt{A_{inc}}}$ for QT specimens (F-QT, G-QT, SCV-QT, SUP-QT, G, GER,

and GVM) is obtained according to the same way as Chapetti. It is found that although the datum points in Fig. 8a are rather scattered, Eq. 4 could be used to describe the relationship between N_f and $\frac{\sqrt{A_{GBF}}}{\sqrt{A_{inc}}}$ for these specimens approximately. As regards the pre-charged specimens, Fig. 8b shows the relationship between N_f and $\frac{\sqrt{A_{GBF}}}{\sqrt{A_{inc}}}$ for specimens SCV-CD1, SCV-CD2, SUP-CD, G-SK1, and G-SK2. It is found that these datum points approximately accord with Eq. 4 as well. Comparing Fig. 8a with b, we might infer that hydrogen charged into specimens by SK and CD charging does not influence the relationship between N_f and $\frac{\sqrt{A_{GBF}}}{\sqrt{A_{inc}}}$ substantially. This phenomenon demonstrates from another point of view that hydrogen charged into steels by SK and CD charging is mainly trapped by reversible traps, such as dislocations etc.; and SK and CD charging do not substantially change the hydrogen amount trapped by inclusions. Since hydrogen trapped by inclusion is a crucial factor in the formation of GBF; therefore, it can influence the GBF size at an identical N_f . It has been reported by Murakami that the ratio of GBF to inclusion size at the identical N_f is smaller

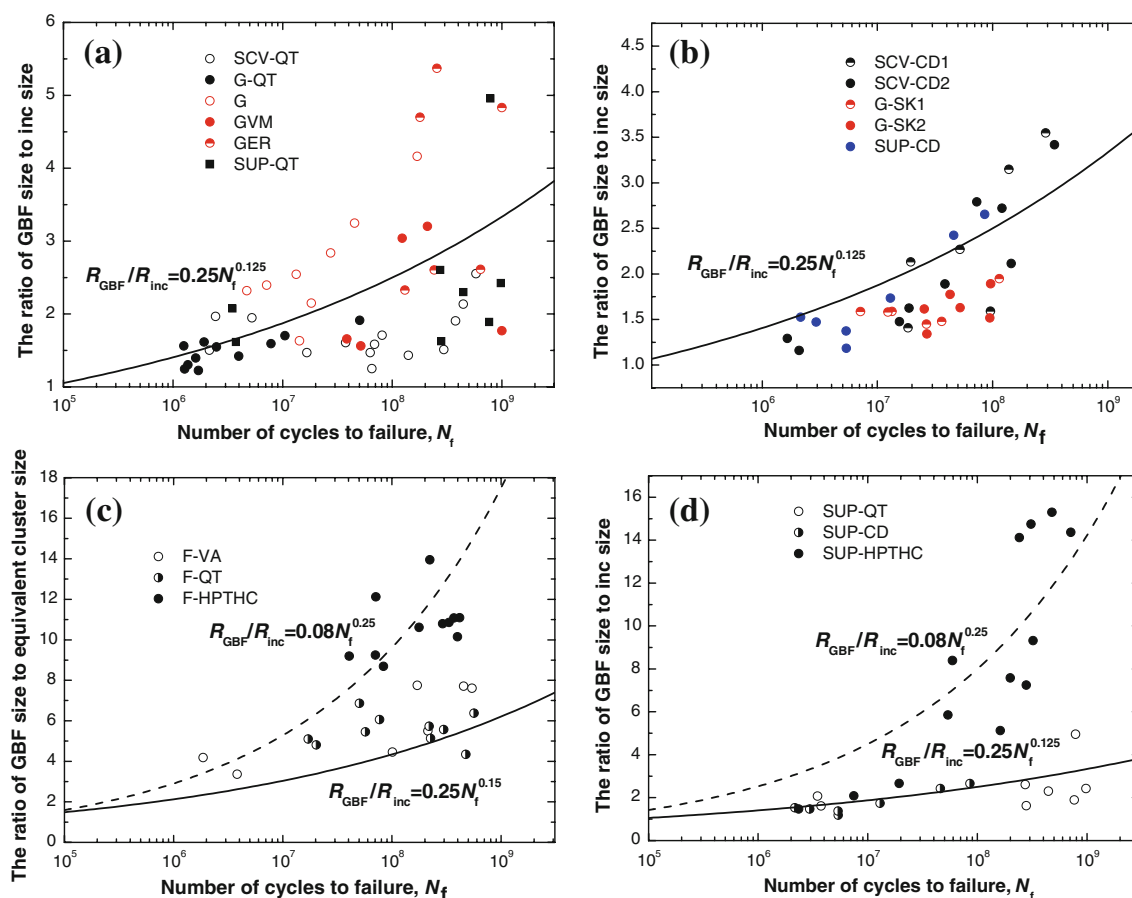


Fig. 8 The relationship between N_f and the ratio of GBF to inclusion size. **a** QT specimens, **b** pre-charged specimens by the cathodic charging and soaking method, **c** F50CrV4 steel (F-VA, F-QT and F-HPTHC) and **d** SUP12 steel (including SUP-QT, SUP-CD and SUP-HPTHC)

in vacuum quenching (VQ) specimens ($C_H = 0.07$ ppm) than in QT ($C_H = 0.8$ ppm) specimens [20].

The relationship between N_f and the ratio of GBF to inclusion size for F50CrV4 steels (F-VA, F-QT, and F-HPTHC) and SUP12 steels (SUP-QT, SUP-CD, and SUP-HPTHC) is illustrated in Fig. 8c, d, respectively. The inclusion size in F50CrV4 steels is so small that it is not easy to be distinguished by SEM; thus, the equivalent inclusion cluster size in Table 4 is used. In Fig. 8c, the ratio of GBF to equivalent cluster size for F-VA and F-QT specimens are rather close, the fitting expression of datum points for specimens F-VA and F-QT is approximately in accordance with Eq. 4, $\frac{\sqrt{A_{GBF}}}{\sqrt{A_{inc}}} = \frac{R_{GBF}}{R_{inc}} = 0.25N_f^{0.15}$, here the power of N_f is slightly increased from 0.125 to 0.15. On the other hand, compared F-HPTHC with F-VA and F-QT specimens, it is obvious that the ratio of GBF to equivalent cluster size for F-HPTHC specimens is much larger than that of F-VA and F-QT specimens. In Fig. 8d, the fitting expression of datum points for SUP-CD and SUP-QT specimens is in accordance with Eq. 4. However, the ratio of GBF to inclusion size for SUP-HPTHC specimens is obviously larger than that of SUP-CD and SUP-QT specimens at the identical N_f . If we fit a curve for SUP-HPTHC and F-HPTHC specimens in the form of Eq. 4— $\frac{\sqrt{A_{GBF}}}{\sqrt{A_{inc}}} = \frac{R_{GBF}}{R_{inc}} = aN_f^b$, then the exponent— b is definitely greater than 0.125, the approximate fitting expression for SUP-HPTHC and F-HPTHC specimens is as follows:

$$\frac{\sqrt{A_{GBF}}}{\sqrt{A_{inc}}} = \frac{R_{GBF}}{R_{inc}} = 0.08N_f^{0.25}. \tag{6}$$

Equation 6 is rewritten as

$$N_f = 2.4 \times 10^4 \left(\frac{R_{GBF}}{R_{inc}} \right)^4. \tag{7}$$

We can find that hydrogen being charged into steels by HPTHC obviously influences the GBF size compared with uncharged specimens. This phenomenon may provide a collateral evidence of the point of view again that hydrogen charged into steels by HPTHC technology is trapped mainly by inclusions [10].

As mentioned above, the GBF size in F-HPTHC and SUP-HPTHC specimens were determined without much difficulty; however, the GBF boundary cannot be distinguished clearly in the SCV-HPTHC specimens, therefore the relationship between N_f and $\frac{\sqrt{A_{GBF}}}{\sqrt{A_{inc}}}$ for specimens SCV-HPTHC cannot be figured out.

The relationship between stress amplitude (σ_a) and fatigue life (N_f) can be usually expressed by Basquin equation

$$\sigma_a = \sigma'_f (2N_f)^b \tag{8}$$

σ'_f is the fatigue strength coefficient, b the Basquin exponent, and $b < 0$. After rearrangement of Eq. 4 and substituting it into Eq. 8, then we obtained

$$\frac{R_{GBF}}{R_{inc}} = 0.23 \left(\frac{\sigma_a}{\sigma'_f} \right)^{\frac{1}{8b}}. \tag{9}$$

Because of $b < 0$, $\frac{R_{GBF}}{R_{inc}}$ will be reduced with the increase of σ_a . Similar situation can be found for the pre-charged specimens.

The stress intensity factor range at the periphery of GBF— ΔK_{GBF}

Based on the model of “effective projective area,” Murakami [21] deduced the expression of ΔK_{GBF} :

$$\Delta K_{GBF} = 0.5\Delta\sigma\sqrt{\pi\sqrt{A_{GBF}}}, \tag{10}$$

where ΔK_{GBF} is in MPa m^{1/2}, $\Delta\sigma$ the stress range (in MPa), and $\sqrt{A_{GBF}}$ the square root of the projected area of the GBF area (in μm). In many references [5, 22, 23], ΔK_{GBF} was calculated and it was considered that ΔK_{GBF} was almost a constant for a certain kind of steels, and that ΔK_{GBF} was independent of loading stress, the size of $\sqrt{A_{GBF}}$ and the number of cycles to failure. In this work, the value of ΔK_{GBF} according to Eq. 10 was calculated for all specimens except SCV-HPTHC specimens.

Figure 9 shows the relationship between the GBF size ($\sqrt{A_{GBF}}$) and the stress intensity factor range at the periphery of the GBF, ΔK_{GBF} , for QT specimens. It can be found that ΔK_{GBF} is not a constant and is not independent of $\sqrt{A_{GBF}}$ but is approximately proportional to $(\sqrt{A_{GBF}})^{1/3}$ through the linear fitting. It seems that ΔK_{GBF} decreases

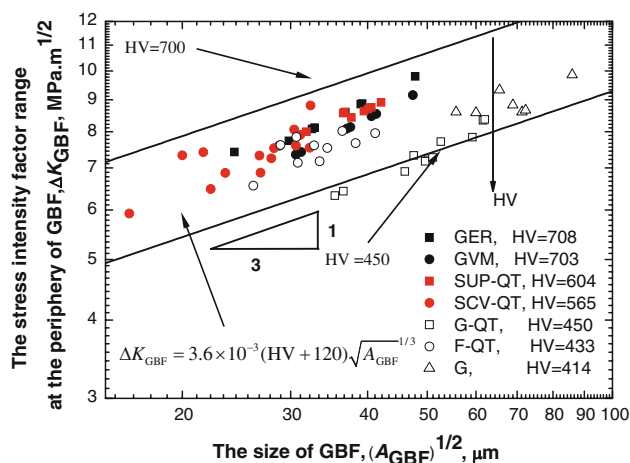


Fig. 9 The relationship between the GBF size— $\sqrt{A_{GBF}}$ and the stress intensity factor range at the periphery of GBF— ΔK_{GBF} for QT specimens

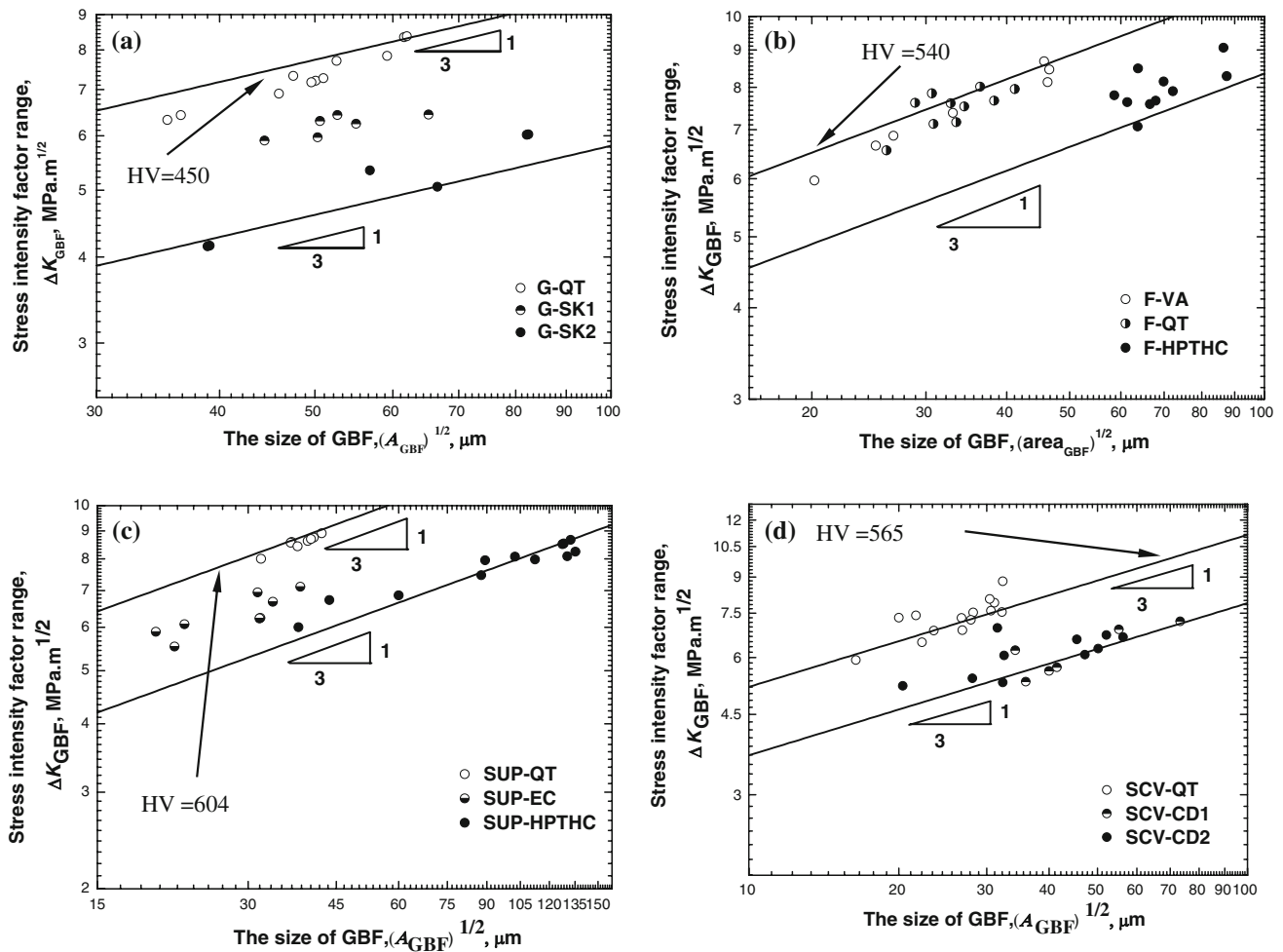


Fig. 10 The relationship between the GBF size— $\sqrt{A_{GBF}}$ and the stress intensity factor range at the periphery of GBF— ΔK_{GBF} for specimens with different hydrogen contents. **a** G50CrV4, **b** F50CrV4, **c** SUP12 and **d** 60Si2CrV

with HV decreasing on the whole. In a recent article of our group [24], we obtained an approximate relationship for uncharged high strength steels as follows:

$$K_{GBF} = 1.8 \times 10^{-3} (HV + 120) \sqrt{A_{GBF}}^{1/3}, \quad (11)$$

that is,

$$\Delta K_{GBF} = 3.6 \times 10^{-3} (HV + 120) \sqrt{A_{GBF}}^{1/3}. \quad (12)$$

In this work, the relationship between $\sqrt{A_{GBF}}$ and ΔK_{GBF} approximately accords with the above expression.

Figure 10 shows the relationship between $\sqrt{A_{GBF}}$ and ΔK_{GBF} for specimens with different hydrogen contents. Like Fig. 9, ΔK_{GBF} is approximately proportional to $(\sqrt{A_{GBF}})^{1/3}$ for each specimen. But it is interesting to note that ΔK_{GBF} decreases with the increase of hydrogen content. This is to say that hydrogen reduces the stress intensity factor range at the periphery of GBF— ΔK_{GBF} . ΔK_{GBF} actually can be considered as the stress intensity factor threshold for a small crack in the vicinity of GBF area, then we can see that the threshold in

the vicinity of GBF decreases with the increase of hydrogen content, namely hydrogen reduces the threshold for a small crack to propagate at the periphery of the GBF. Therefore, crack can propagate under a lower stress. This is may be one of the reasons why pre-charged specimens can fail in a much lower stress than non-charged specimens. From Figs. 9 and 10, we can find that ΔK_{GBF} could approximately be a constant when $\sqrt{A_{GBF}}$ is in a small range; so, ΔK_{GBF} was usually considered as a constant in many articles; however, it is found that ΔK_{GBF} is not a constant but is approximately proportional to $(\sqrt{A_{GBF}})^{1/3}$ when more steels were investigated and $\sqrt{A_{GBF}}$ is in a large range (10–100 μm).

Conclusions

1. The modified Murakami’s fatigue strength expression is validated to be effective for hydrogen pre-charged and uncharged high strength steels.

2. The ratio of GBF to inclusion size for pre-charged specimens by HPTHC is greater than that for SK and CD charging as well as uncharged specimens.
3. The stress intensity factor range at the periphery of the GBF, ΔK_{GBF} , is approximately proportional to $(\sqrt{A_{\text{GBF}}})^{1/3}$. ΔK_{GBF} decreases with the increase of hydrogen content no matter which hydrogen charging method is used.

Acknowledgement This work was financially supported by key project of basic research of China (2004CB619100). The authors wish to thank Prof. L. J. Rong, Dr. J. Zhang, and Prof. G. Y. Li for their useful advice and experimental supports.

References

1. Yang ZG, Li SX, Zhang JM, Li GY, Li ZB, Hui WJ, Weng YQ (2004) *Acta Mater* 52:5235
2. Murakami Y, Nomoto T, Ueda T (2000) *Fatigue Fract Eng Mater Struct* 23:893
3. Murakami Y, Nomoto T, Ueda T (2000) *Fatigue Fract Eng Mater Struct* 23:903
4. Murakami Y (2002) *Metal fatigue: effects of small defects and nonmetallic inclusions*. Elsevier, Amsterdam & Boston, p 273
5. Shiozawa K, Lu L, Ishihara S (2001) *Fatigue Fract Eng Mater Struct* 24:781
6. Shiozawa K, Morii Y, Nishino S, Lu L (2006) *Int J Fatigue* 28:1521
7. Yang ZG, Li SX, Liu YB, Li YD, Li GY, Hui WJ, Weng YQ (2008) *Int J Fatigue* 30:1016
8. Garet M, Brass AM, Haut C, Guttierrez-Solana F (1998) *Corros Sci* 40:1073
9. Oriani RA, Hirth JP, Smialowski M (1985) *Hydrogen degradation of ferrous alloys*. Noyes Publ, Park, Ridge
10. Li YD, Yang ZG, Li SX, Liu YB, Chen SM, Hui WJ, Weng YQ (2009) *Adv Eng Mater* 11(7):561
11. Li YD, Yang ZG, Li SX, Li SX, Li GY, Hui WJ, Weng YQ (2008) *Mater Sci Eng A* 498:373
12. Yang ZG, Zhang JM, Li SX, Li GY, Wang QY, Hui WJ, Weng YQ (2006) *Mater Sci Eng A* 427:167
13. Murakami Y (2002) *Metal fatigue: effects of small defects and nonmetallic inclusions*. Elsevier, Amsterdam & Boston, p 94
14. Oriani RA, Hirth JP, Smialowski M (1985) *Hydrogen degradation of ferrous alloys*. Noyes Publ., Park Ridge, p 718
15. Onyevuanyi OA, Hirth JP (1981) *Scr Met* 115:113
16. Chapetti MD, Tagawa T, Miyata T (2003) *Mater Sci Eng A* 356:236
17. Bathias C (1999) *Fatigue Fract Eng Mater Struct* 22:559
18. Murakami Y (2002) In: *Proceeding of the eighth international fatigue congress (Fatigue 2002)*, EMAS Ltd., vol 5, p 2927
19. Murakami Y, Yokoyama NN, Kenichi T (2001) *J Soc Mater Sci Jpn* 50(11):1068
20. Murakami Y, Yokoyama NN, Nagata J (2002) *Fatigue Fract Eng Mater Struct* 25:735
21. Murakami Y (2002) *Metal fatigue: effects of small defects and nonmetallic inclusions*. Elsevier, Amsterdam & Boston, p 17
22. Sakai T, Sato Y, Oguma N (2002) *Fatigue Fract Eng Mater Struct* 25:765
23. Nakajima M, Kamiya M, Itoga H, Tokaji K, Ko HN (2006) *Int J Fatigue* 28:1540
24. Liu YB, Yang ZG, Li YD, Chen SM, Li SX, Hui WJ, Weng YQ (2008) *Mater Sci Eng A* 497:408